Journal of
Synchrotron
Radiation

ISSN 0909-0495

Received 13 February 2004
Accepted 5 January 2005

On the influence of the incident photon energy on the radiation damage in crystalline biological samples

Manfred S. Weiss,* Santosh Panjikar, Christoph Mueller-Dieckmann and Paul A. Tucker

EMBL Hamburg Outstation, c/o DESY, Notkestrasse 85, D-22603 Hamburg, Germany.
E-mail: msweiss@embl-hamburg.de

Two series of complete and highly redundant data sets were collected at wavelengths of 1.00 and 2.00 Å on a cadmium derivative of porcine pancreatic elastase (PPE). Radiation damage to the sample was evaluated qualitatively by inspecting consecutive difference electron density maps during the course of the experiment. The nature of the radiation damage was found to be identical at both wavelengths and was localized primarily at the four disulfide bridges of PPE, the cadmium site and the two methionine residues. For a quantitative examination of the radiation damage, the decrease in the peak height of the cadmium ion in various electron density maps was exploited. Again, no significant difference in radiation damage between the two wavelengths was observed. This can be rationalized by considering the wavelength dependencies of the number of diffracted photons *versus* the number of absorbed photons and the energy deposited in the crystal by the latter.

Keywords: radiation damage; photoelectric absorption; coherent scattering; X-ray crystallography; long wavelength; disulfide bond.

1. Introduction

Radiation damage occurring to crystalline biological macromolecules while under investigation by X-ray diffraction always limits the quality and the quantity of structural information that can be obtained from one crystal as it puts a limit on the number of incident photons or the amount of absorbed energy the crystal can stand. With the introduction and the extensive use of cryocrystallographic methods into biological X-ray crystallography about a decade ago, the problem seemed to have become less and less important. However, the advent of third-generation synchrotron sources with their bright and small X-ray beams has forced the community to realise that, even inside a crystal imbedded in vitreous ice at 100 K, radiation damage is occurring, and that it is occurring to an extent that imposes severe constraints on the way in which an experiment may be performed (Gonzalez & Nave, 1994).

The advent of radiation damage is directly related to the values for the cross sections for photoelectric absorption, coherent scattering and incoherent scattering (Fig. 1). The dominating primary event at all photon energies typically used in macromolecular crystallography is the production of a photoelectron by photoelectric absorption. The photoelectron then travels through the crystal and causes further damage. When diffraction data are collected at 100 K, a temperature at which the solvent mixture inside the crystal is vitrified, secondary events will only involve damage by electrons. Damage by radical species produced by electrons should not be significant, because the radicals are not able to diffuse inside the vitreous ice.

Since the values for the various cross sections are dependent on the incident photon energy, radiation damage also influences the choice of the wavelength for collecting diffraction data. At shorter wavelengths, absorption is less of a problem and, consequently, radiation damage should be less severe. In contrast, longer wavelengths provide an increase in scattered intensity, and they may therefore be superior in this respect. The scattering efficiency, however, which is defined as the number of diffracted photons divided by the energy deposited in the crystal, appears to call for the shorter wavelengths again. There are a number of papers which address this issue (Arndt, 1984; Polikarpov, 1997; Polikarpov *et al.*, 1997; Teplyakov *et al.*, 1998) although with sometimes conflicting conclusions. The situation will again be different if crystal size or detector efficiency become an issue, or if the ratio of anomalous signal *versus* deposited dose has to be optimized. For MAD/SAD data to be collected, the wavelength(s) have to be chosen according to which elements are present in the crystal, but for some other applications, in which anomalous signals are exploited, experiments conducted at wavelengths in the 2.0 Å range appear to yield the largest signal-to-noise

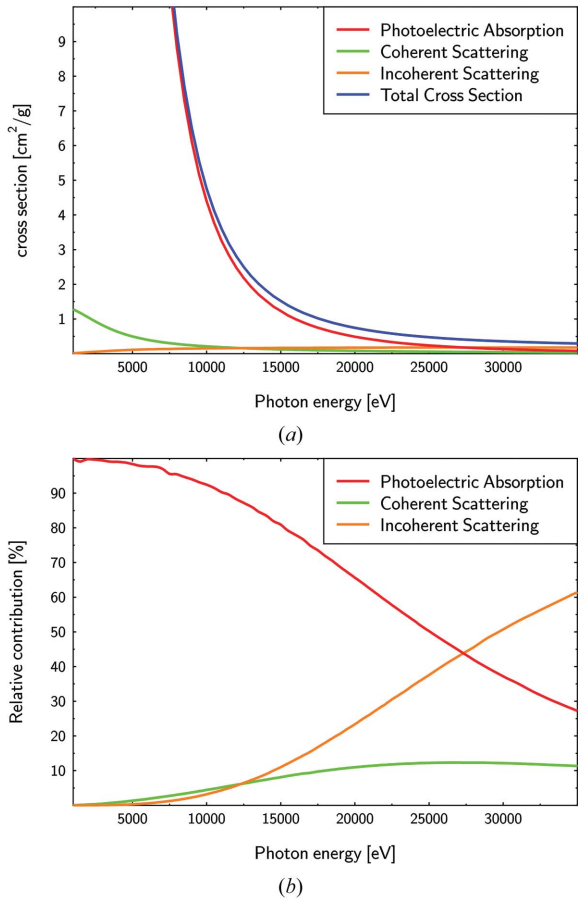

Figure 1
Dependence of the cross sections for photoelectric absorption, coherent scattering and incoherent scattering on the incident photon energy. (*a*) Absolute values, (*b*) relative contributions. The values were calculated using the XCOM server (http://physics.nist.gov/PhysRefData/Xcom/Text/XCOM.html) at NIST (Gaithersburg, MD, USA) based on the composition of an average protein crystal (9% H, 27% C, 8% N, 55% O and 1% S).

ratio (Weiss *et al.*, 2001; Mueller-Dieckmann *et al.*, 2004; Djinovic Carugo *et al.*, 2005).

Historically, radiation damage to protein crystals has either been neglected altogether or described using only two parameters to explain overall reduction of the scattering power of the crystal as a function of the incident X-ray dose. More recently, it has been realised that radiation damage to a macromolecule inside a crystal bears some elements of site specificity (Weik *et al.*, 2000) with disulfide bonds being the major susceptible sites. The observation that specific radiation damage can be induced in protein molecules by synchrotron radiation even led to the formulation of the concept of radiation-damage-induced phase determination (RIP) (Ravelli *et al.*, 2003). Phase determination by RIP is based on two diffraction data sets collected before and after a high-dose exposure, which is required to introduce the specific damage. In this method the changes, owing to radiation damage, within a particular data set are assumed to be negligible. For the cases in which severe radiation damage already occurs during the collection of one data set, there have also been attempts to correct for the specific radiation damage by extrapolating the observed intensities to their value at zero dose (Diederichs *et al.*, 2003), but this in turn requires the data being collected with a greater than fourfold redundancy.

The diffraction experiments which are most sensitive to radiation damage are experiments that rely on the exploitation of anomalous scattering for phase determination. Usually the anomalous signal, which can be derived from a diffraction experiment, is a small difference between two experimentally determined large numbers, which makes a carefully designed experiment a *conditio sine qua non*. Radiation damage will further reduce the anomalous signal by destroying the anomalously scattering substructure and it will also alter the signal by modifying the substructure. This will be especially detrimental for experiments which utilize the tiny anomalous signal provided by sulfur and phosphorus atoms present in native protein and nucleic acid molecules for phase determination. These experiments require a very high data redundancy in order to improve the otherwise low signal-to-noise ratio (Dauter & Adamiak, 2001; Weiss, 2001). In addition, the high data redundancy may also provide the basis for the removal of some systematic errors from the data. Recently, the use of longer X-ray wavelengths (λ = 1.5–3.0 Å) has been advocated in order to enhance these small signals (Weiss *et al.*, 2001; Helliwell, 2004; Djinovic Carugo *et al.*, 2005; Mueller-Dieckmann *et al.*, 2004), but measuring diffraction data at longer wavelengths has also raised the question as to whether radiation damage will be enhanced at these wavelengths.

The purpose of this study is now to investigate whether there is an influence of the data-collection wavelength on the radiation damage to the crystalline sample in both a qualitative and quantitative sense. The model system chosen is a cadmium complex of porcine pancreatic elastase (PPE) and the wavelengths investigated are 1.00 Å and 2.00 Å, both far away from the absorption edges of any of the elements present in the crystal.

2. Materials and methods

2.1. Crystallization

Commercially available PPE (Serva, Product No. 20929, Lot No. 15448) was used for crystallization without further purification. The protein was dissolved in deionized water to a concentration of 20 mg ml^{-1}. Crystals of the Cd^{2+} complex of PPE were grown in a similar fashion to those of the Ca^{2+} complex of PPE (Weiss *et al.*, 2002). The reservoir solution contained 100 m*M* sodium acetate buffer at pH 5.1, 200 m*M* sodium citrate and 20 m*M* $CaCl_2$, whereas in the drop solution the $CaCl_2$ was replaced by 40 m*M* $CdCl_2$. A 1:1 (*v*/*v*) mix of the drop solution and the protein solution was then equilibrated at 293 K using a vapour-diffusion hanging-drop set-up. These conditions yield crystals of the Cd complex of PPE in a couple of days. The crystals belong to space group $P2_12_12_1$ with unit-cell dimensions of a = 50.0 Å, b = 57.8 Å and c = 74.3 Å. They diffract X-rays to better than 1.0 Å resolution.

2.2. Data collection

Diffraction data sets were collected at the X-ray diffraction beamline at the ELETTRA Synchrotron Radiation Facility (Trieste, Italy) using a MARCCD detector with a diameter of 165 mm. Two crystals of PPE/Cd^{2+} of similar size ($\sim$200 µm × 200 µm × 200 µm) were used. From the first crystal (crystal A), 180° of data were collected at λ = 1.00 Å as a reference data set (A-0) followed by twelve times 360° at λ = 1.00 Å (data sets A-1 to A-12). Each data set was collected as a series of 1° images with approximate exposure times of about 6–7 s per image. Care was taken to avoid the recording of overloaded reflections on the detector so that complete data sets could be obtained in one sweep. From the second crystal (crystal B), 180° of data were also collected at λ = 1.00 Å as a reference data set (B-0), which was then followed by eight times 360° at λ = 2.00 Å (B-1 to B-8). Here, the approximate average exposure time per image was about 3 s. For all data sets the maximum resolution has been limited to 1.85 Å by setting the crystal–detector distance to 132 mm (at λ = 1.00 Å) and 36 mm (at λ = 2.00 Å). The total time that the crystal was exposed to X-rays amounted to approximately 7.5 h for crystal A, which very roughly corresponds to a dose of about 5×10^6 Gy, based on the equation given by O'Neill *et al.* (2002), a flux of about 10^{12} photons s^{-1} at λ = 1.00 Å in a 1.2 mm × 2.0 mm beam (see http://www.elettra.trieste.it/experiments/beamlines/xrd1) and a crystal size of about 200 µm × 200 µm × 200 µm. For crystal B, which was exposed to X-rays for about 2.6 h, the corresponding number would be two-thirds of the value of crystal A, assuming that the flux at λ = 2.00 Å is only about half of that at λ = 1.00 Å, which is consistent with the observed readings in the ionization chamber closest to the crystal (IC2). In the absence of reliable flux measurements, however, these numbers have to be taken with extreme caution.

2.3. Data processing

All data sets were indexed and integrated using *DENZO* (Otwinowski & Minor, 1997). The post-refinement procedure in *SCALEPACK* (Otwinowski & Minor, 1997) was used to refine the cell parameters and the mosaicity for each data set. For scaling and merging, the program *SCALA* (Collaborative Computational Project, Number 4, 1994) was used with the scaling model *SCALA-Abs* as described by Mueller-Dieckmann *et al.* (2004). At first, different scale and temperature factors were refined for each image, with the temperature factors of neighboring images being restrained to similar values. In a second scaling run, the scale factors were allowed to vary as a function of the secondary beam direction in crystal coordinates expanded in spherical harmonics. The redundancy-independent merging *R*-factor, $R_{\rm r.i.m.}$, as well as the precision-indicating merging *R*-factor, $R_{\rm p.i.m.}$ (Weiss, 2001), were calculated using the program $R_{\rm merge}$ (available upon request from MSW or from http://www.embl-hamburg.de/~msweiss/projects/msw_qual.html). The relevant data-processing parameters are given in Tables 1(*a*) and 1(*b*). Finally, structure factor amplitudes were calculated from intensities using the program *TRUNCATE* (Collaborative Computational Project, Number 4, 1994).

Table 1
Relevant data-processing statistics of (*a*) data sets A-0 to A-12 and (*b*) data sets B-0 to B-8.

Data set	$d_{\rm min}$ (Å)	$I/\sigma(I)$	$R_{\rm merge}$ (%)	$R_{\rm p.i.m.}$ (%)	$R_{\rm anom}$ (%)	Overall *B*-factor (Å^2)†
(*a*)						
A-0	1.85	66.3 (40.1)	2.2	0.9	1.2	13.2
A-1	1.85	81.5 (48.2)	2.6	0.7	1.0	13.3
A-2	1.85	81.0 (47.5)	2.6	0.7	1.0	13.5
A-3	1.85	83.8 (49.2)	2.5	0.7	1.0	13.7
A-4	1.85	84.1 (48.4)	2.6	0.7	1.0	13.7
A-5	1.85	87.0 (50.4)	2.5	0.7	1.0	13.8
A-6	1.85	87.4 (50.7)	2.4	0.7	1.0	14.1
A-7	1.85	86.9 (50.2)	2.5	0.7	1.0	14.2
A-8	1.85	86.4 (49.6)	2.5	0.7	1.0	14.4
A-9	1.85	85.7 (48.9)	2.5	0.7	1.0	14.5
A-10	1.85	84.7 (48.0)	2.5	0.7	1.0	14.7
A-11	1.85	85.7 (48.4)	2.5	0.7	1.0	14.9
A-12	1.85	83.8 (46.7)	2.5	0.7	1.0	15.0
(*b*)						
B-0	1.85	54.4 (27.1)	2.5	1.1	1.2	11.9
B-1	1.85	42.8 (22.4)	5.1	1.6	2.5	14.2
B-2	1.85	43.3 (22.6)	5.1	1.5	2.5	14.4
B-3	1.85	42.7 (22.2)	5.1	1.5	2.4	14.5
B-4	1.85	41.8 (21.5)	5.1	1.6	2.4	14.7
B-5	1.85	40.9 (21.0)	5.3	1.6	2.4	14.9
B-6	1.85	39.3 (19.7)	5.4	1.7	2.4	15.1
B-7	1.85	39.0 (19.6)	5.4	1.7	2.4	15.2
B-8	1.85	38.8 (19.4)	5.4	1.7	2.4	15.4

† From Wilson plot as calculated using *TRUNCATE* (Collaborative Computational Project, Number 4, 1994).

2.4. Assessment of radiation damage

In order to assess the influence of radiation damage, the structure of the PPE Cd complex was first refined against data sets A-0 and B-0 starting from the coordinate set 1LKB (Weiss *et al.*, 2002) and using the program *REFMAC* (Collaborative Computational Project, Number 4, 1994). The structure refined against data set A-0 (R = 16.49%, $R_{\rm free}$ = 20.48%) contained all 240 amino acids of PPE, one Cd^{2+}, one Cl^-, one CH_3COO^-, one glycerol and 222 water molecules. The structure and the corresponding data set have been deposited with the PDB (entry 1UVO). The structure refined against data set B-0 (R = 16.61%, $R_{\rm free}$ = 21.19%) contained all 240 amino acids of PPE, one Cd^{2+}, one Cl^-, one CH_3COO^-, one glycerol and 229 water molecules. The structure and the corresponding data set have also been deposited with the PDB (entry 1UVP). Using the phases derived from these models, difference Fourier syntheses were calculated based on the coefficients $(F_{\rm A\text{-}y} - F_{\rm A\text{-}1})$ with y = 2–12 and $(F_{\rm B\text{-}x} - F_{\rm B\text{-}1})$ with x = 2–8 to obtain a qualitative picture of the site specificity of the radiation damage as it occurred. For a more quantitative analysis, the procedure described by Mueller-Dieckmann *et al.* (2004) was applied. The Cd^{2+} ion was omitted from the refined structures and the remaining coordinates refined against all other 360° data sets in order to use the reduction of the absolute cadmium peak height in the $(2F_{\rm obs} - F_{\rm calc}, \alpha_{\rm calc})$ map,

the ($F_{obs} - F_{calc}$, α_{calc}) map, as well as the anomalous difference Fourier ($F^{+}_{obs} - F^{-}_{obs}$, $\alpha_{calc} - 90^{\circ}$) map as an indicator of radiation damage. In all cases the refinement was conducted in the resolution range 20.0–1.85 Å.

3. Results and discussion

3.1. Data collection

The aim was to make full use of the dynamic range of the detector and to collect all data sets with no overloaded reflections. This way it was possible to collect all low- and high-resolution reflections in one sweep. Based on the readings in IC2, the number of incident photons per image or per data set is about twice as high for the A data sets as for the B data sets (Table 2). This was necessary to utilize the full dynamic range of the MARCCD detector at both data-collection wavelengths. Because of absorption and air scatter, this also leads to exposure times per image which are about twice as long for the A data sets than for the B data sets. Since the diffracted intensity is proportional to λ^2 (Drenth, 1999), the number of diffracted photons per image should therefore be approximately equal in both cases.

Table 2
Relative data collection, diffraction and absorption parameters for data sets A and B.

	Wavelength (λ) dependence	Data sets A (λ = 1.00 Å)	Data sets B (λ = 2.00 Å)
Relative IC2 readings†	λ^2	1	2
No. of photons impinging on the crystal	–	2	1
No. of photons impinging on the crystal per image	–	4	1
No. of diffracted photons per image	λ^2	1	1
No. of photons absorbed by the crystal per image	λ^3	1	2
Energy deposited in crystal per image	λ^2	1	1

† IC2 is the second ionization chamber after the last pair of slits and closest to the crystal.

3.2. Quality of the data sets

The quality of all data sets as described by the merging statistics given in Tables 1(*a*) and 1(*b*) is exceptionally good. The high redundancy of about 13 to 16 observations per reflection in each data set leads to very small $R_{p.i.m.}$ values, *i.e.* low noise levels in the data. If one compares the data sets A-0 and B-0 it becomes clear, however, that the diffraction power of crystal B is about 20–30% lower than that of crystal A. This is most likely due to a somewhat smaller crystal volume of crystal B, a notion which is also corroborated by the observed difference in scale factors (7.4 for crystal A and 15.4 for crystal B) when placing the scaled and merged intensities on an approximate absolute scale in the program *TRUNCATE* (Collaborative Computational Project, Number 4, 1994). Since the diffracted intensities are proportional to the square of the crystal volume, the difference in scale factors indicates a volume ratio of about 1.0 to 0.7 (crystal A *versus* crystal B). Overall, the B data sets exhibit lower $I/\sigma(I)$ values and higher R_{merge} and $R_{p.i.m.}$ values than the A data sets. The reasons for this are (i) the smaller volume of crystal B as noted above, and (ii) the insufficient correction of absorption by the scaling protocol used. Similar behavior has been noted previously (Mueller-Dieckmann *et al.*, 2004). There is only very little change of the merging statistics as a function of the data-collection time (Table 1), which indicates that radiation damage is occurring only very gradually and is not degrading the data quality within a single data set to any significant extent. The overall temperature factors derived from the respective Wilson plots corroborate this notion. Even though they are increasing steadily, the absolute increase is only about 0.15 Å^2 per data set. Furthermore, the increase per data set is the same at both wavelengths (A-1 to A-8 and B-1 to B-8). It is interesting to note in this respect that the Wilson *B*-factors of data sets B-0 and B-1 are significantly different (Table 1*b*). Since a 200 µm-thick protein crystal of average composition $C_{125}H_{508}N_{34}O_{191}S_1$ and average density 1.2 g cm^{-3} exhibits a transmission of only about 0.6 at a wavelength of λ = 2.00 Å (see http://www-cxro.lbl.gov/optical_constants/filter2.html), it is likely that the scaling procedure employed (see §2.3) is not able to fully correct for the absorption effects occurring at λ = 2.00 Å.

3.3. Qualitative nature of radiation damage

The qualitative nature of the radiation damage occurring can be assessed by the difference Fourier syntheses ($F_{A\text{-}12} - F_{A\text{-}1}$, α_{calc}) and ($F_{B\text{-}8} - F_{B\text{-}1}$, α_{calc}). The positive density (shown in green in Fig. 2) depicts the density that is appearing during the course of the experiment, and the negative density (shown in red in Fig. 2) shows the electron density that is disappearing as a consequence of radiation damage. The sites which are most susceptible to radiation damage are, in order of decreasing susceptibility, SS-bridge Cys158–Cys174 > SS-bridge Cys30–Cys46 > SS-bridge Cys127–Cys194 $\simeq$ SS-bridge Cys184–Cys214 > Cd^{2+} ion > Met172 > Met41. With a correlation coefficient of 0.77 between the two difference electron density maps shown in Fig. 2, it can be concluded that qualitatively there is no difference in radiation damage at different incident photon energies. When the difference electron density map ($F_{B\text{-}8} - F_{B\text{-}1}$, α_{calc}) is compared with the ($F_{A\text{-}8} - F_{A\text{-}1}$, α_{calc}) map, the observed correlation coefficient (0.78) is even slightly higher, although the difference is probably too small to be significant. It should be noted, however, that the two incident photon energies considered in this experiment are far from any absorption edges of either sulfur or cadmium. The outcome of a similar experiment may well be different if one or both of the two incident photon energies are close to an absorption edge, because around an absorption edge the discontinuity in the anomalous scattering length (and therefore the absorption cross section) will result in vastly different deposited doses. Particularly at the site of the absorbing element, significantly more photons should be absorbed at the peak of the $\Delta f''$ curve, potentially resulting in more site-

specific damage. In our experiment, even though the $\Delta f''$ values for both Cd or S are significantly different between the two wavelengths, the ratio $\Delta f''$(Cd)/$\Delta f''$(S) stays approximately the same, which may explain the similar distribution of the damage.

3.4. Quantitative assessment of radiation damage

Quantitatively, radiation damage was assessed by inspecting the peak height of the Cd^{2+} ion site in various electron density maps in a similar fashion to that carried out for the Xe peak height by Mueller-Dieckmann *et al.* (2004). The decrease of the Cd^{2+} peak height in the $(2F_{obs} - F_{calc}, \alpha_{calc})$ map, in the $(F_{obs} - F_{calc}, \alpha_{calc})$ map and in the anomalous difference Fourier $(F^{+}_{obs} - F^{-}_{obs}, \alpha_{calc} - 90^{\circ})$ map is shown in Fig. 3. It is very difficult to estimate, however, to what extent the Cd^{2+} sites are damaged specifically, and to what extent the reduction in peak height is a consequence of the overall radiation damage as indicated by the Wilson *B*-factors (Table 1), especially in the light of the fact that also the Met-SD atoms and the water molecules exhibit a similar decrease in their peak height in the $(2F_{obs} - F_{calc}, \alpha_{calc})$ map. Nevertheless, the picture all three maps provide is nicely consistent. Even when comparing the two different wavelengths used, the decrease of the cadmium peak height is very similar.

By making a few very rough assumptions about the wavelength dependence of the beamline ionization chamber response, the absorption and scattering events, the observation of the identical extent of damage can be rationalized in a fairly crude manner (Table 2). Similar arguments have already been put forth by Arndt (1984) and Gonzalez & Nave (1994). As discussed above, the number of photons on the crystal per data set is about twice as high for crystal A than for crystal B. Taken together with the difference in exposure times per image, this leads to an approximately equal number of diffracted photons per image. However, the number of photons absorbed by the crystal is proportional to λ^3. This means that, per image, about twice the number of photons were absorbed in crystal B and, given the fact that the energy of a 2.0 Å-wavelength photon is only half that of a 1.0 Å-wavelength photon, the total energy deposited in the crystal should be about equal in both cases (see also the estimation of the dose values in §2.2). Therefore, it is not surprising to find that the radiation damage is also equal. It should be stressed that this reasoning is only valid far away from any absorption edge of elements present in the crystal and it is also important to note that the rationalization given is per diffraction image and not per unit exposure time.

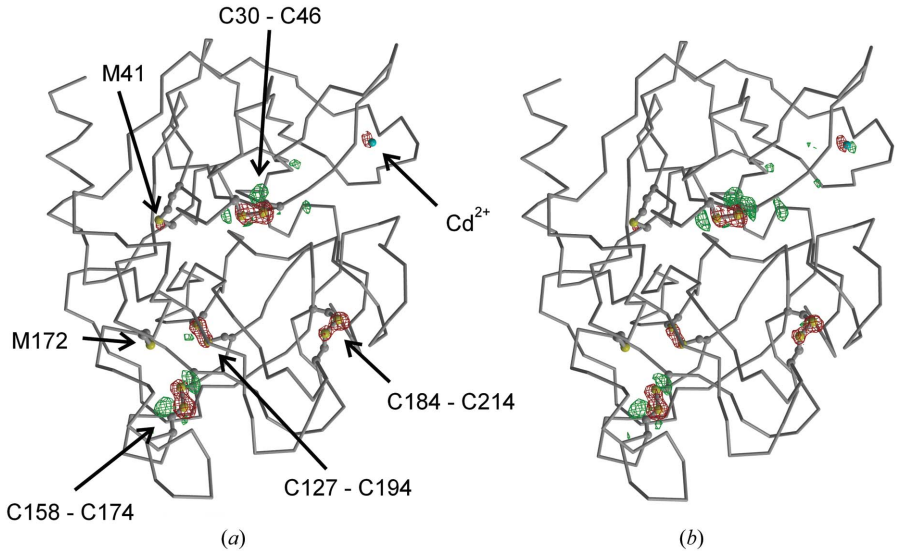

Figure 2
The nature of radiation damage in PPE/Cd^{2+}. The nature of the radiation damage in (*a*) the A data sets and (*b*) the B-data sets as exemplified by difference Fourier syntheses with the coefficients $(F_{A\text{-}12} - F_{A\text{-}1})$ and $(F_{B\text{-}8} - F_{B\text{-}1})$. The phases used were derived from the models refined against data sets A-0 and B-0. Shown is the positive electron density contoured at five standard deviations above the mean in green, and the negative electron density contoured at five standard deviations below the mean in red. The figure was produced using the programs *MOLSCRIPT* (Kraulis, 1991), *BOBSCRIPT* (Esnouf, 1997) and *RASTER3D* (Merritt & Bacon, 1997).

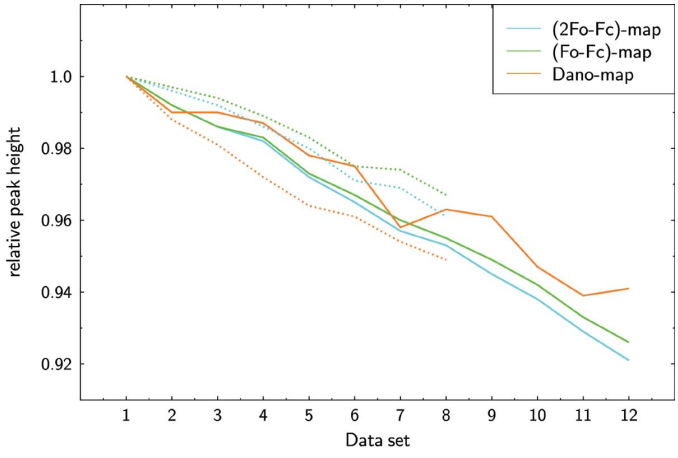

Figure 3
Quantitative assessment of radiation damage in PPE/Cd^{2+}. Depicted is the decrease of the relative cadmium peak height $(2F_{obs} - F_{calc}, \alpha_{calc})$ maps (blue), the $(F_{obs} - F_{calc}, \alpha_{calc})$ maps (green) as well as the anomalous difference Fourier $(F^{+}_{obs} - F^{-}_{obs}, \alpha_{calc} - 90^{\circ})$ maps (brown) of data sets A-1 to A-12 (solid lines) and data sets B-1 to B-8 (broken lines). All peak heights were scaled to the values found in data set A-1.

4. Summary and conclusions

At different incident photon energies far from any absorption edges of elements present in the crystal, radiation damage appears to be indistinguishable both qualitatively and quantitatively. However, some of the assumptions which had to be made to rationalize this observation are only roughly valid. For a better and a more quantitative assessment of what is really happening, it is obligatory that in future experiments a well calibrated pin diode is used to obtain accurate flux

measurements, that the size and the shape of the crystal as well as the surrounding mother liquor is recorded, and that the wavelength dependence of the detector response is taken into account.

We would like to thank the staff of the X-ray diffraction beamline at ELETTRA (Trieste, Italy) for beam time and their support. We also acknowledge the support of this work by the EC 5th Framework Programme 'Transnational Access to Major Research Infrastructures' (Contract No. HPRI-CT-1999-00033) and the Deutsche Forschungsgemeinschaft (DFG grant WE2520/2 to MSW).

References

Arndt, U. W. (1984). *J. Appl. Cryst.* **17**, 118–119.
Collaborative Computational Project, Number 4 (1994). *Acta Cryst.* D**50**, 760–763.
Dauter, Z. & Adamiak, D. A. (2001). *Acta Cryst.* D**57**, 990–995.
Diederichs, K., McSweeney, S. & Ravelli, R. B. G. (2003). *Acta Cryst.* D**59**, 903–909.
Djinovic Carugo, K., Helliwell, J. R., Stuhrmann, H. & Weiss, M. S. (2005). *J. Synchrotron Rad.* **12**. In the press.
Drenth, J. (1999). *Principles of Protein X-ray Crystallography*, 2nd ed., p. 103ff. Heidelberg: Springer-Verlag.
Esnouf, R. M. (1997). *J. Mol. Graph.* **15**, 132–134.
Gonzalez, A. & Nave, C. (1994). *Acta Cryst.* D**50**, 874–877.
Helliwell, J. R. (2004). *J. Synchrotron Rad.* **11**, 1–3.
Kraulis, P. J. (1991). *J. Appl. Cryst.* **24**, 946–950.
Merritt, A. E. & Bacon, D. J. (1997). *Methods Enzymol.* **277**, 505–524.
Mueller-Dieckmann, C., Polentarutti, M., Djinovic Carugo, K., Panjikar, S., Tucker, P. A. & Weiss, M. S. (2004). *Acta Cryst.* D**60**, 28–38.
O'Neill, P., Stevens, D. C. & Garman, E. F. (2002). *J. Synchrotron Rad.* **9**, 329–332.
Otwinowski, Z. & Minor, W. (1997). *Methods Enzymol.* **276**, 307–326.
Polikarpov, I. (1997). *J. Synchrotron Rad.* **4**, 17–20.
Polikarpov, I., Teplyakov, A. & Oliva, G. (1997). *Acta Cryst.* D**53**, 734–737.
Ravelli, R. B., Leiros, H. K., Pan, B., Caffrey, M. & McSweeney, S. (2003). *Structure*, **11**, 217–224.
Teplyakov, A., Oliva, G. & Polikarpov, I. (1998). *Acta Cryst.* D**54**, 610–614.
Weik, M., Ravelli, R. B., Kryger, G., McSweeney, S., Raves, M. L., Harel, M., Gros, P., Silman, I., Kroon, J. & Sussman, J. L. (2000). *Proc. Natl. Acad. Sci. USA*, **97**, 623–628.
Weiss, M. S. (2001). *J. Appl. Cryst.* **34**, 130–135.
Weiss, M. S., Panjikar, S., Nowak, E. & Tucker, P. A. (2002). *Acta Cryst.* D**58**, 1407–1412.
Weiss, M. S., Sicker, T. & Hilgenfeld, R. (2001). *Structure*, **9**, 771–777.